Inflammatory monocytes promote perineural invasion via CCL2-mediated recruitment and cathepsin B expression

Richard L. Bakst[1], **Huizhong Xiong**[2,#], **Chun-Hao Chen**[3], **Sylvie Deborde**[3], **Anna Lyubchik**[3], **Yi Zhou**[3], **Shizhi He**[3], **William McNamara**[3], **Sei-Young Lee**[3], **Oakley C. Olson**[5], **Ingrid M. Leiner**[2], **Andrea R. Marcadis**[3], **James W. Keith**[2], **Hikmat A. Al-Ahmadie**[4], **Nora Katabi**[4], **Ziv Gil**[6], **Efsevia Vakiani**[4], **Johanna A. Joyce**[5,7], **Eric Pamer**[2], and **Richard J. Wong**[3]

[1]Department of Radiation Oncology, Mount Sinai School of Medicine, New York, NY 10029
[2]Immunology Program, Memorial Sloan-Kettering Cancer Center, New York, NY 10065
[3]Department of Surgery, Memorial Sloan Kettering Cancer Center, New York, NY 10065
[4]Department of Pathology, Memorial Sloan Kettering Cancer Center, New York, NY 10065
[5]Cancer Biology and Genetics Program, Memorial Sloan Kettering Cancer Center, New York, NY 10065 [6]Department of Otolaryngology, Rambam Healthcare Campus, The Technion-Israel Institute of Technology, Haifa, Israel [7]Ludwig Institute for Cancer Research, University of Lausanne, CH-1066 Lausanne, Switzerland

Abstract

Perineural invasion (PNI) is an ominous event strongly linked to poor clinical outcome. Cells residing within peripheral nerves collaborate with cancer cells to enable PNI but the contributing conditions within the tumor microenvironment are not well understood. Here we show that CCR2-expressing inflammatory monocytes (IM) are preferentially recruited to sites of PNI, where they differentiate into macrophages and potentiate nerve invasion through a cathepsin B-mediated process. A series of adoptive transfer experiments with genetically engineered donors and recipients demonstrated that IM recruitment to nerves was driven by CCL2 released from Schwann cells at the site of PNI, but not CCL7, an alternate ligand for CCR2. Interruption of either CCL2-CCR2 signaling or cathepsin B function significantly impaired PNI *in vivo*. Correlative studies in human specimens demonstrated that cathepsin B producing macrophages were enriched in invaded nerves, which was associated with increased local tumor recurrence. These findings deepen our understanding of PNI pathogenesis and illuminate how PNI is driven in part by corruption of a nerve repair program. Further, they support the exploration of inhibiting IM recruitment and function as a targeted therapy for PNI.

Keywords

perineural invasion; inflammatory monocyte; macrophages; pancreatic cancer; cathepsin

Introduction

Perineural invasion (PNI), the local extension of cancer along nerves, is an ominous finding in many solid tumors that is closely linked to poor clinical outcomes (1–3). Despite widespread acknowledgement of the adverse clinical significance of PNI, the mechanisms underlying its pathogenesis remain largely unknown and specific therapies targeting nerve invasion are lacking. Modern theories of PNI pathogenesis have placed significant focus on the role of the nerve microenvironment with PNI resulting from well-orchestrated interactions between cancer and the nerve (2, 3). While the cellular components of the nerve microenvironment are relatively static and well defined under homeostasis, PNI develops within a dynamic and complex tumor microenvironment that is enriched with immune cells recruited from the circulation (4, 5) and whose contribution to nerve invasion is unclear. Our knowledge gap in this area stems in part from the inability of *in vitro* PNI models to recapitulate the immune milieu, and the lack of consistent and quantifiable nerve invasion with current *in vivo* tumor models (6).

PNI was traditionally viewed as a cancer-driven event. Our group more recently has demonstrated that the nerve (7, 8), and the cells that reside within it including Schwann cells (9) and endoneurial macrophages (10) contribute to PNI by cancer. Endoneurial macrophages represent a subset of tissue-resident macrophages that inhabit normal peripheral nerves, which are distinct from the hematogenous macrophages that are derived from monocytes recruited under various pathological conditions (11). In tumors with a strong predilection for PNI such as pancreatic ductal adenocarcinoma (PDA) (1), the microenvironment is enriched with monocytes and macrophages from the circulation, which contribute to PDA tumorigenesis (12) and negatively mediate disease progression and local invasion (4, 5). While there is strong evidence that recruited inflammatory monocytes (IM) may promote distant metastases (13, 14), the potential contribution of recruited IM towards the progression of cancer along nerves is unclear. CCR2, a chemokine receptor expressed on IM, has an established role in monocyte recruitment (15). CCL2 and CCL7 bind to CCR2 on IM and drive their recruitment following infection and inflammation (15, 16). However, the respective contributions of CCL2 versus CCL7 in driving IM recruitment to cancer niches remain obscure (13). Prior investigation of the CCL2 signaling axis in PNI focused on the role of cancer cell CCR2-expression (17), and therefore very little is known about the contributions of IM towards nerve invasion.

Interestingly, IM are also recruited to nerves following traumatic injury where they differentiate into macrophages and cultivate a growth permissive microenvironment allowing for nerve repair (11). We hypothesized that this conserved monocyte response to nerve injury may be induced by invading cancer cells to inadvertently promote PNI. Macrophages are detected in regions of PNI by PDA and their presence is associated with poor clinical outcome (5, 6, 10, 18). However, despite appreciation of their clinical relevance, we currently have a limited understanding of their origin, recruitment mechanism, and function within nerves. There is strong rationale to study the role of IM in mediating this ominous process especially in light of evidence that CCR2 is important for macrophage accumulation within nerves and in turn PNI. Here we investigate the contribution, recruitment mechanism, and downstream functions of IM towards promoting PNI.

Materials and Methods

Patient cohorts

Samples from paraffin-embedded human specimens (n = 23 PDA, n = 5 benign pancreas, n = 18 prostate adenocarcinoma, and n = 10 adenoid cystic carcinoma) were retrieved from the archives of Memorial Sloan-Kettering Cancer Center, New York, NY, USA. All specimens were collected from previous surgical resections at our institution according to standard procedures. Memorial Sloan-Kettering Cancer Center Institutional Review Board approved studies on human tissue samples (Protocol # 15-052). Written informed consent was received from the patients. Patient studies were conducted in accordance with the ethical guidelines of the Belmont Report.

Tissue preparation and immunohistochemistry

At indicated times after injection, murine sciatic nerves were dissected up to the spinal cord and were fixed using 4% paraformaldehyde and embedded in paraffin. Sections from human pancreatic, prostate and adenoid cystic carcinoma specimens were obtained from paraffin blocks that were prepared using a standard protocol. For immunofluorescence, all sections were permeabilized and blocked in 3% horse serum, 0.1% Triton X-100/PBS for 1 hour. Primary antibodies diluted in 0.1% horse serum/PBS were incubated overnight at 4°C. Sections were washed with PBS and detection was performed using first and an appropriate fluorescent secondary Ab (AlexaFluor 488, Alexa Fluor 568 at 1:500, Invitrogen). For anti-cathepsin B and anti-CD68 co-expression on human samples, automatic Particle counting in Image J was performed to identify individual cells. The number of green/red/orange cells was recorded in corresponding channels, and the percentage of co-stained cells (orange) among total green or red cells was calculated and subsequent manual confirmed. CTSB score was calculated by dividing the total number of CTSB positive cells by the number of DAPI positive cells within a region of PNI. Scores were then averaged per specimen. Image J was also used to quantify the intensity of Collagen IV staining. The intensity was calculated as the raw intensity (RawIntDen)-Area X Background intensity, and reverted to positive values.

Reagents, small molecule inhibitors and antibodies

The following primary antibodies were used for immunofluorescence staining at the indicated dilutions: anti-GFAP (1:1000, Dako, Z033429-2), anti-F4/80 (1:50, Abcam, AB6640), human anti-Cathepsin B (1:1000, R&D, AF953), murine anti-Cathepsin B (1:500, R&D, AF965), human anti-CD68 (1:1, Dako, PG-M1), and murine anti-CD68 (1:3000, Serotec, FA-11). The following primary antibodies were used for IHC at the indicated dilutions: human anti-CD163 (1:200, Vector, 10D6), human anti-CD68 (1:200, Dako, M0876), anti-collagen IV (1:200, Vector labs, PK6101), murine anti-GFP (1:100, Abcam, AB1218), and human anti-CCR2 (1:400, Novus biologicals, E68). JPM-OEt (100 mg/kg/day) was administered intraperitoneally in 30% DMSO/70% PBS as previously described (19).

Mouse strains

Nude mice and C57BL/6J mice were obtained from The Jackson Laboratory. *Ccl2* KO (15), *Ccl7* KO (15), *Ccr2* KO (20), CCL2-GFP (21), and CCR2-GFP (22) have all been previously described and were provided by the Pamer laboratory. *Ctsb* KO (23, 24) and *Ctss* KO (24, 25) have been previously described and were provided by the Joyce laboratory.

Cell culture

MiaPaCa-2 was purchased from ATCC. The murine cell line Panc02 was from Dr. Min Li (26). The murine cell line KPC was from Dr. Vonderheide (27). Cell line authentication was performed using short tandem repeat profiling. The cell lines tested negative for mycoplasma contamination. Cells were cultured in 5% CO_2 at 37°C in Dulbecco's modified Eagle's medium (DMEM, Cellgro, Herndon, VA) containing 10% fetal bovine serum (Gemini, Woodland, CA) and 50 U/ml penicillin/streptomycin (Cellgro, Herndon, VA).

Enzyme-linked immunosorbent assays (ELISA)

Sciatic nerves underwent homogenization with an electronic pestle grinder (Fisher Scientific, Pittsburgh, PA). Tissue lysates were then centrifuged. CCL2, CCL7, and CCL3 levels were assessed using the mCCL2 ELISA Kit (BD Biosciences), CCL-7/MCP-3 Instant ELISA Kit (BD Biosciences), and MIP-1 alpha/CCL3 ELISA Kit (eBioscience), respectively.

FACS analysis and antibodies

For FACS analysis, spleen, femoral bone marrow and sciatic nerves were washed in cold PBS following collection, and then spleens and nerve specimens were minced on ice and digested with an enzyme mix of Collagenase IV (Worthington) at 37°C for 40 minutes to obtain single-cell suspensions. Antibodies were purchased from BD Bioscience unless otherwise indicated. The following clones were used: anti-Ly6C (AL-21), Ly6G (1A8), CD11b (M1/70), CD45 (30F-11), F4/80 (BM8), CD45.1 (A20), CD45.2 (104), CD90 (53-2.1), p75 (EMD Millipore, AB1554) and CD11c (HL3). FACS analysis was performed on a LSRII cytometer (BD Biosciences) and data analyzed using Flowjo software (TreeStar). Where specified, a ratio of IM in the nerve specimen was normalized to those in the spleen to account for potential differences in the circulation between mice.

Adoptive cell transfer

CD45.1[+] GFP[+] bone marrow monocytes from CCR2-GFP[+] mice (22) were sorted from femoral bone marrow and adoptively transferred into the following mice: nude athymic mice, WT C57BL/6J mice, CCL2 KO mice, and CCL7 KO mice. 10^6 cells were intravenously transferred into mice bearing sciatic nerve at the time points specified by the individual experiments. CD45.2^{+} CD11b^{+} Ly6C^{+} bone-marrow monocytes were sorted from both WT CD45.2 C57BL/6J mice and CD45.2 CCR2 KO mice, and adoptively transferred into a CD45.1 C57BL/6J mice bearing sciatic nerve tumors in a similar manner. For all experiments, mice were sacrificed 18 hours following adoptive transfer unless otherwise specified and the specimens analyzed via FACS. For the rescue experiment, 10^6 GFP[+] bone marrow monocytes from CCR2-GFP[+] mice were transferred into CCR2 KO mice

undergoing sciatic nerve injection mice at three separate time intervals (days 1, 5, 8) and sacrificed on day 11.

RNA and quantitative real-time PCR

The desired cell type was sorted from *in vivo* tumor samples unless otherwise specified. Total RNA was extracted using the Trizol reagent according to the manufacturer's protocol (Ambion RNA, Life Technologies). Aliquots of 1 μg of total RNA were transcribed using QuantiTect Reverse Transcription Kit (QIAGEN). PCR and fluorescence detection were performed using the StepOnePlus Sequence Detection System (Applied Biosystems) according to the manufacturer's protocol in a reaction volume of 20 μl containing 1× TaqMan Universal PCR Master Mix (Applied Biosystems) and 30 ng cDNA. For quantification of mouse *Ccl2*, *CTSB*, and *CTSS* mRNA, Thermo Scientific DyNAmo Flash Probe qPCR Kit was used. All measurements were performed in duplicates and the arithmetic means of the cycle threshold (Ct) values were used for calculations: target gene mean Ct values were normalized to the respective housekeeping gene β-actin, mean Ct values (internal reference gene, Ct), and then to the experimental control.

Animal experiments

Sciatic nerve injections were performed as previously described (8). Equal volumes of cancer cells were injected into the flank when indicated. Sample sizes were chosen based on previous published literature with this nerve model. Briefly, all mice were anesthetized using isoflurane (1–3%), and their sciatic nerve was exposed. MiaPaCa-2 (150,000 cells), Panc02 (50,000 cells), or KPC (50,000 cells) were injected into the sciatic nerve under using a custom Hamilton syringe. All experiments contained a biological (or control) replicate arm. When indicated, an equivalent volume of sterile PBS was injected into the nerve as a control. No randomization method was utilized to assign treatment groups as all mice were of the same sex, age and genetic background. Mice were excluded only if no primary tumor could be found after cancer cell implantation, otherwise all subjects were included in the analysis. Sciatic nerve function was assessed using the nerve function score (28). It was graded according to hind limb paw response to manual extension of the body, from 4 (normal) to 1 (total paw paralysis). At the indicated times after injection, mice were sacrificed and the sciatic nerves were dissected up to the spinal cord. Length of invasion was measured up from the proximal edge of the primary tumor up to the most distal portion of the thickened nerve using calipers. Tumor volume was calculated based the formula, 4.18 x (length/2) x (width/2)^2. When comparing PNI versus flank specimens, tumor mass was assessed to account for variance in tumor shapes. Animal studies were conducted in accordance to the Memorial Sloan-Kettering Institutional Animal Care and Use Committee (Protocol # 05-04-006).

Statistical analysis

Statistical analysis was conducted using an unpaired, two-tailed Student's t-test and Mann Whitney test. The number of technical replicates for each experimental arm is indicated in the respective figure legends. Statistical significance was defined as $P < 0.05$.

Results

Monocytes Selectively Accumulate in Nerves with PNI and Differentiate Into Macrophages

To investigate a potential role of IM in PNI, we measured monocyte trafficking utilizing a validated murine model of PNI (Fig. 1A left) (8, 28). Although the sciatic nerve model does not allow for the slow neural remodeling seen in human PDA (29), it has the advantage of preserving the nerve microenvironment while providing reliable clinical and pathological endpoints for nerve invasion. Human pancreatic cancer cells, MiaPaCa2, were injected into the distal sciatic nerves of athymic nude mice. Murine monocytes were identified by fluorescence-activated cell sorting (FACS) from sciatic nerve specimens with and without PNI. Endogenous IM, defined by high expression of both Ly6C and CD11b, were detected at high frequency within invaded nerves (Supplementary Fig. S1) but rarely present in normal nerves (Fig. 1A right, B).

We then sorted GFP$^+$ IM from CCR2-GFP donors, and adoptively transferred these IM into recipient mice following sciatic nerve injection with MiaPaCa2 or PBS as a control. Eighteen hours after adoptive transfer, GFP$^+$ cells were preferentially recruited to the site of PNI (Fig. 1C,D), and were readily detectable along the invaded nerve via immunohistochemistry (IHC) (Fig. 1E). A noticeable fraction of GFP$^+$ cells, isolated only from PNI specimens, already started to differentiate into F4/80$^+$ CD11b$^+$ mature macrophages by 18 hours post transfer. This differentiation was not observed in other organs where transferred IM had infiltrated (Fig. 1F), suggesting that the local nerve microenvironment was driving their maturation. To confirm the fate of the transferred wild type (WT) IM after downregulation of CCR2/GFP during differentiation, we performed adoptive transfer of WT CD45.2 IM into CD45.1 WT mice following cancer cell injection. By day three, the majority of transferred cells isolated from the invaded nerves, but not the spleen, had differentiated into F4/80$^+$ CD11b$^+$ macrophages (Fig. 1G,H). To evaluate the role of tumor tissue in mediating monocyte recruitment, we performed sciatic nerve and flank Panc02 injections and compared respective IM and macrophage quantities. We identified significantly more IM and macrophage accumulation in the PNI specimens as compared to the flank specimens (Supplementary Fig S1), highlighting the fundamental importance of the nerve microenvironment in mediating monocyte recruitment. Analysis of human pancreatic samples with anti-CD163 staining confirmed the selective accumulation of macrophages around nerves invaded by PDA in comparison to intrapancreatic nerves from benign pancreatic specimens where macrophages were rarely observed (Fig. 1I,J). Collectively, these findings demonstrate a preferential recruitment of IM from the circulation to nerves with PNI where they are driven to differentiate into macrophages.

Loss of CCR2 Impairs IM Recruitment to the Nerve and Reduces PNI In Vivo

To study the mechanisms involved in IM homing to nerves with PNI, we performed cancer cell injections into the sciatic nerve of CCR2 KO mice using Panc02. Mice were followed clinically after injection using a validated sciatic nerve score to assess nerve function (4=full function, 1=complete paralysis) (8, 28). At the time of sacrifice, the length of nerve invasion was also measured to determine the extent of PNI. CCR2 KO mice had significantly better nerve function (Fig. 2A) and reduced nerve invasion (Fig. 2B,C and Supplementary Fig S2)

in comparison to WT mice. Nerve specimens from CCR2 KO mice had a significant reduction in the amount of IM (Fig. 2D,E) and macrophages (Fig. 2F,G) suggesting that their recruitment promotes PNI. The IM number was further normalized to the spleen of the same individual animal because the spleen is a peripheral reservoir for IM and an indicator of their availability in the peripheral circulation (20). Even when accounting for the differences in the availability of IM in the circulation, the local reduction of IM in CCR2 KO mice still persisted compared to WT (Fig. 2E right), suggesting contribution of CCR2 to IM homing to the nerve. Cancer cell injection of a second murine pancreatic cancer cell line, KPC, into CCR2 KO mice resulted in clinical, pathological and FACS findings similar to that of Panc02 (Supplementary Fig. S2). Importantly, Panc02 and KPC tumor volumes were comparable in both WT and CCR2 KO mice (Supplementary Figs. S2 and S3), suggesting that the observed nerve invasion reduction in CCR2 KO mice was due to impaired monocyte recruitment rather than diminished tumor growth.

To confirm the importance of CCR2 in IM recruitment to the nerve, we adoptively transferred equivalent numbers of CD45.2 CCR2 KO IM or CD45.2 WT IM into CD45.1 WT mice with nerve invasion (Fig. 2H left). At 18 hours following transfer, there was a significant reduction in both the absolute and the relative number of CCR2 KO IM compared to WT IM in nerves with invasion, (Fig. 2H right) indicating that IM expression of CCR2 is integral to IM recruitment to the nerve. To examine the function of CCR2^{+} IM in PNI development, we performed a rescue experiment with three sequential transfers of WT IM into a cohort of CCR2 KO mice. WT IM transfer accelerated PNI development in CCR2 KO mice, and the degree of clinical and pathologic nerve invasion was comparable to that of WT mice (Fig. 2I and Supplementary Fig. S4). Consistent with this phenotype, the quantity of macrophages detected in the invaded nerves of CCR2 KO mice receiving IM increased to the endogenous levels found in the WT cohort (Fig. 2J and Supplementary Fig. S4).

Loss of CCL2, not CCL7, Impairs PNI In Vivo

CCL2 plays a role in IM recruitment to distant metastatic sites (13). To determine potential contributions of CCL2 to PNI, we assessed the nerve invasion model in CCL2 KO mice using Panc02. In comparison to WT mice, CCL2 KO mice had significantly better nerve function (Fig. 3A) and reduced nerve invasion (Fig. 3B,C and Supplementary Fig. S5). This correlated with a significant reduction in both IM (Fig. 3D,E) and macrophage quantities (Fig. 3F) in CCL2 KO nerve specimens. Cancer cell injection of a second murine pancreatic cancer cell line, KPC, into CCL2 KO mice resulted in similar clinical, pathological and FACS findings (Supplementary Fig. S3). To confirm that this effect was related to IM recruitment, we performed an adoptive transfer of GFP-labeled WT monocytes into CCL2 KO recipients following Panc02 injection (Fig. 3G). There was a significant reduction in GFP-labeled cells isolated from the nerve specimens from CCL2 KO mice on FACS analysis, even when normalized to the splenic population, suggesting that local nerve CCL2 production is directly involved in IM recruitment.

CCL7 is an alternate ligand for CCR2 that can influence IM recruitment (15, 30). To assess its role, we again utilized our nerve invasion model in CCL7 KO mice. Unlike CCL2 KO mice, CCL7 KO mice developed paralysis and invasion comparable to WT mice (Fig. 3H–J).

Consistently, nerve specimens from CCL7 KO mice demonstrated a slight and non-significant decrease in IM and macrophages (Fig. 3K–M) which likely reflect secondary, indirect effects of reduced IM availability in the peripheral circulation as demonstrated by a reduction in splenic IM (Supplementary Fig. S5). Furthermore, we performed adoptive transfer of WT IM into both CCL2 KO and CCL7 KO mice. CCL2 KO mice had significantly fewer IM isolated from the nerve as compared with CCL7 KO mice, underscoring the key role of CCL2, but not CCL7, in IM homing to invaded nerves (Fig. 4A).

Schwann Cell Secretion of CCL2 Drives IM Recruitment to Sites of PNI

We investigated whether chemokines were produced locally in the invaded nerve by performing CCL2 and CCL7 enzyme-linked immunosorbent assays (ELISA) on nerve specimens from WT, CCL2 KO, and CCL7 KO mice following Panc02 injection. CCL2 was detected in both WT and CCL7 KO mice (Fig. 4B). By contrast, CCL7 was undetectable in all cohorts potentially accounting for its lack of clinical relevance in our model. We also assayed for CCL3 in nerves with PNI given that it can be trigged by CCL2 release (31), however, it was undetectable by ELISA (Supplementary Fig. S6). To identify the cellular source of CCL2, we performed cancer cell injections into the sciatic nerves of CCL2-GFP reporter mice (21). GFP expression, reflecting CCL2 production, was detected only in regions of nerve invasion (Fig. 4C). Because Schwann cells recruit IM in the setting of peripheral nerve injury (32), we hypothesized that Schwann cells may be the cellular source of CCL2. We performed immunofluorescence staining with anti-GFP and anti-GFAP, an activated Schwann cell marker (33), on nerve specimens from CCL2-GFP reporter mice following cancer cell injection. GFP expression by GFAP positive spindle shaped cells adjacent to areas of nerve invasion was detected, suggestive of Schwann cells (Fig. 4D). Dissociated nerve specimens with and without cancer invasion were then sorted by FACS to isolate p75+ Schwann cells and Panc02 cells for RT-PCR to assess relative *Ccl2* expression. The p75+ Schwann cells significantly upregulated *Ccl2* in the presence of cancer invasion, although the Panc02 cells showed low expression of *Ccl2* (Fig. 4E). To test the therapeutic effect of blocking local CCL2 production on PNI, we treated mice with anti-CCL2 antibody or with a control antibody following Panc02 injection. Anti-CCL2 treatment significantly reduced nerve invasion (Fig. 4F) and showed a corresponding reduction in local nerve CCL2 levels and IM recruitment (Fig. 4G and Supplementary Fig. S7) without any observed systemic side effects.

Cathepsin B Produced by Recruited Macrophages Promotes PNI in Mice

IM differentiate into macrophages after being recruited to the nerves (Fig. 1F–H). Macrophages are known to be able to enhance the ability of cancer to invade and metastasize through a variety of mechanisms (34). To explore mechanisms through which macrophages may facilitate PNI, we performed a RT-PCR based screen from recruited macrophages isolated from the murine PNI specimens for a number of established macrophage-derived growth factors and proteases known to promote cancer growth and invasion (Supplementary Table 1). Macrophages isolated from non-tumor bearing sites served as comparisons to identify candidates potentially enriched in PNI pathogenesis. Among the candidates, there was abundant and differential expression of both cathepsin B and S but not other cathepsin

proteases (Fig. 5A). To determine if cysteine cathepsins were involved in promoting PNI, we performed a therapeutic trial using a pan-cathepsin inhibitor, JPM-OEt (19). Treatment of mice with JPM-OEt significantly reduced nerve invasion in comparison to DMSO-treated controls (Fig. 5B,C).

We then sought to identify the host-derived cathepsins involved in facilitating PNI. Based on the differential expression patterns observed in our initial RT-PCR screen, we hypothesized that cathepsin B (CTSB) and/or cathepsin S (CTSS) may be most relevant. We performed sciatic nerve injections of Panc02 cells into both CTSB KO and CTSS KO mice. CTSS KO mice did not show any significant reduction in clinical or pathological PNI (Fig. 5D,E). However, CTSB KO mice exhibited significantly improved nerve function (Fig. 5F) and reduced nerve invasion (Fig. 5G,H) and with similar tumor volumes (Supplementary Fig. S8) as compared to control WT mice. To determine if macrophages were the predominant source of CTSB, we performed *Ctsb* RT-PCR on FACS sorted Panc02, IM and macrophages from invaded nerve specimens. Macrophages demonstrated the highest level of *Ctsb* mRNA, suggesting that they were the predominant cellular source of CTSB (Fig. 5I) in the PNI model. To confirm this finding and determine if CTSB was produced in the proximity of invaded nerves, we performed anti-cathepsin B and anti-F4/80 staining on invaded nerves, and detected co-staining within cells in regions of PNI (Fig. 5J).

Cathepsin B can promote invasion by cancer through a number of mechanisms including degradation of extracellular matrix, cleavage of cellular adhesion molecules, and activation of pro-angiogenic signaling (35). We performed a histological screening of proteins degraded by CTSB and also known to be important components of the perineurium: laminin (36, 37), fibronectin (38, 39), and collagen IV (40, 41). No discernible differences in staining patterns were appreciated in PNI specimens from CTSB KO mice (vs. WT) for laminin or fibronectin (data not shown). However, collagen IV, an integral component of the protective perineurium (40) was notably disrupted in WT mice with PNI but not in CTSB KO specimens (Fig. 5K). In such samples, CTSB-expressing macrophages were detected adjacent to regions of collagen IV irregularity in WT mice with PNI (Supplementary Fig. S9).

Alteration of the Perineurium is Associated with Cathepsin B Expressing Macrophages in Human Tumors

Macrophages are present within or adjacent to the majority of nerves invaded by human PDA (Fig. 6A) as well as other solid tumor histologies with a predilection for PNI (Supplementary Figs. S10 and S11). We analyzed clinical outcomes in our PDA cohort (Supplementary Table 2) and observed a significantly higher proportion of PNI foci infiltrated by macrophages in patients who developed a local recurrence (Supplementary Fig. S12), a finding that supports prior work showing an adverse clinical impact of macrophage infiltration around nerves in PDA (5). To determine if macrophage-produced CTSB is relevant in promoting PNI by PDA in patients, we co-stained human PDA samples with anti-CD68 and anti-cathepsin B. In regions adjacent to areas of PNI, the majority of cathepsin B-positive cells also stained positive for anti-CD68, and the majority of CD68 positive cells also stained positive for cathepsin B (Fig. 6B,C), suggesting that macrophage-

derived CTSB may be relevant in PNI by PDA. To evaluate this, we analyzed clinical outcomes and observed significantly higher CTSB expression in regions of PNI from patients that developed a local recurrence (Supplementary Figs. S13). We then performed anti-collagen IV staining on human pancreatic specimens. Notably, the outer collagen IV layer was disrupted (Fig. 6D) and the intensity of anti-collagen IV staining was significantly diminished in nerves with PNI by PDA in comparison to nerves from benign pancreatic tissue (Fig. 6E). In such regions of diminished staining, CTSB-expressing macrophages were also detected (Fig. 6F).

Discussion

There is a growing appreciation that an aberrant response by the nerve microenvironment supports PNI. Here we identify a nerve-triggered innate immune response, which inadvertently promotes PNI by cancer (Fig. 7). We demonstrate that CCL2, but not CCL7, released by Schwann cells is critical towards the recruitment of IM to the invaded nerve. Once recruited, the IM differentiate into macrophages, which enable PNI. Mechanistically, this is supported at least in part through CTSB production by macrophages, which may disrupt the collagen IV within the perineurium, impairing its function as a protective barrier around the nerve.

The concept that nerves support cancer progression (42) and invasion represented a paradigm shift in our understanding of PNI pathogenesis. This notion spurred investigations of cell types that reside within the nerve including endoneurial macrophages (10) and Schwann cells (9), but neglected contributions from cells which are recruited to nerves under pathological stress. These new findings implicate CCL2-CCR2 mediated IM recruitment as a key event in the local dissemination of cancer along nerves and identify IM-derived macrophages as critical effector cells of this process. Our data suggests that Schwann cells serve as a key source for IM recruitment in PNI. In studies of nerve repair following injury, Schwann cells are also the predominant source of CCL2, which recruits IM to the site of nerve damage (43). In light of recent evidence that Schwann cells promote cancer invasion through NCAM-dependent cancer cell contact and dispersion (9), our current findings highlight the dynamic interplay amongst cells within the microenvironment to inadvertently facilitate nerve invasion (44). Notably, *in vivo* studies of human tumors have demonstrated that cancer cells can also release CCL2 (4, 13). The stimuli that trigger cancer CCL2 secretion are not fully understood, although in pancreatic cancer this may occur in response to treatment (45). While our data support other evidence from nerve repair studies showing that Schwann cells are an important source of CCL2, nerve invasion develops within the context of a complex tumor microenvironment in which there may be additional cellular sources of CCL2 that vary as a function of disease progression and treatment.

Interestingly, our data suggests that CCL7 does not play a critical role in IM recruitment to sites of PNI. There is a paucity of data evaluating the role of CCL7 signaling for IM recruitment in neoplastic settings. Extrapolating from studies of bacterial infection in which deletion of *Ccl7* reduces IM accumulation by up approximately 40–50% (15), we anticipated a contribution of CCL7 signaling on PNI. We observed non-significant reductions in IM from CCL7 KO nerve specimens, which were likely secondary to retention in the marrow

given the parallel reductions we observed in the spleen. Furthermore, we did not detect any local CCL7 production from invaded nerves, a finding that is consistent with the lack of clinical relevance by CCL7 in our model. Interestingly, CCL7 does not appear to play a significant role in IM recruitment following trauma nerve injury either (43), suggesting that IM recruitment in PNI may follow similar recruitment pathways as nerve injury. While the role of CCL7 warrants further investigation in different oncologic settings, this study suggests that the role of CCL7 in IM recruitment for PNI is largely overshadowed by CCL2.

CTSB is a protease with strong associations to cancer progression (35) but not previously linked to PNI. Peripheral and autonomic nerves are ensheathed in a number of protective concentric layers to shield them from injury (46). By definition, PNI represents cancer entry into and along nerves, either breaching or tracking along the perineurium (3). The potential ability of CTSB released by macrophages to disrupt the integrity of the perineurium may represent one plausible explanation of how IM recruitment facilitates PNI. Following peripheral nerve injury, recruited macrophages represent the main effector cells in Wallerian degeneration, the process that results when a nerve fiber is injured, and are programmed to produce a number of proteases in order to clear the traumatic nerve debris to facilitate regrowth (47). Therefore it is plausible to consider that the upregulation of CTSB we observed in recruited macrophages may be the result of a conserved neural regeneration program, which may degrade components of the protective perineurium and facilitate cancer progression. A similar paradigm exists in the central nervous system where cathepsins have been shown to play crucial roles in promoting invasion through degradation of key proteins comprising the blood-brain barrier (48).

The invasion and spread of cancer along nerves promotes local recurrence of tumors. In our cohort, patients who developed a local recurrence had a significantly higher number of macrophages around PNI foci and increased CTSB expression at these regions. Although our patient sample size was small, these findings are supported by larger studies powered to evaluate clinical outcome. Monocyte mobilization (4), macrophage recruitment (5) and CTSB expression (49) have all independently been associated with poor clinical outcome in human PDA. Specifically, high CTSB levels have been correlated with local recurrence following complete surgical resection in a large cohort of pancreatic cancer patients (49), further implicating CTSB in facilitating nerve invasion. Collectively this suggests that the infiltration of CTSB expressing macrophages around invaded nerves may be clinically relevant in human PDA and increase local tumor recurrence.

Currently there are no targeted therapies for PNI. This study suggests that therapeutic targeting of monocyte recruitment and macrophage function may represent strategies to prevent or treat PNI. Given the growing interest in myeloid cell involvement in cancer progression and other disease states, therapeutically targeting their recruitment through interruption of CCL2-CCR2 signaling has been an area of active drug discovery with a number of agents already available (50–52). Importantly, CCR2 inhibition can be safely incorporated into current standard chemotherapy regimens for cancers such as PDA suggesting that this strategy can be tested clinically as a targeted therapy for PNI (53). The identification of macrophages around invaded nerves in both prostate adenocarcinoma and adenoid cystic carcinoma specimens, in addition to PDA, suggests that a strategy of blocking

CCL2-CCR2 signaling may be relevant to a spectrum of solid cancers that exhibit a proclivity for nerve invasion. Therapeutically targeting PNI can have a number of potential benefits including mitigating associated neuropathic pain, improving the feasibility of gross total resection in certain tumors, and/or reducing metastasis. Achieving these effects might collectively result in improved clinical outcomes.

This work advances our conceptual understanding of PNI pathogenesis by demonstrating that an aberrant systemic immune response contributes to what was thought to be a process largely driven by interactions between cancer and the cellular components of a peripheral nerve. Although macrophage activity has been associated with cancer progression, we only more recently have begun to appreciate their role in PNI. Here we develop a model proposing macrophage origin, recruitment, and downstream function in PNI, and present a strategy to therapeutically target their activity. We identify Schwann cell mediated IM recruitment as an important mediator of PNI and implicate macrophage-derived CTSB in this process. Therapeutic strategies that inhibit IM recruitment by targeting CCL2 and CCR2, but not CCL7, as well as macrophage function and CTSB activity should be explored as novel therapies to inhibit PNI. These findings suggest that conserved neural regeneration mechanisms are exploited by cancer to facilitate nerve invasion and demonstrate that the boundary for cell types involved in PNI extends beyond peripheral nerve borders.

Supplementary Material

Refer to Web version on PubMed Central for supplementary material.

Acknowledgments

References

1. Bapat AA, Hostetter G, Von Hoff DD, Han H. Perineural invasion and associated pain in pancreatic cancer. Nature reviews Cancer. 2011; 11:695–707. [PubMed: 21941281]

2. Amit M, Na'ara S, Gil Z. Mechanisms of cancer dissemination along nerves. Nature reviews Cancer. 2016; 16:399–408. [PubMed: 27150016]

3. Bakst RL, Wong RJ. Mechanisms of Perineural Invasion. Journal of neurological surgery Part B, Skull base. 2016; 77:96–106.

4. Sanford DE, Belt BA, Panni RZ, Mayer A, Deshpande AD, Carpenter D, et al. Inflammatory monocyte mobilization decreases patient survival in pancreatic cancer: a role for targeting the CCL2/CCR2 axis. Clinical cancer research : an official journal of the American Association for Cancer Research. 2013; 19:3404–15. [PubMed: 23653148]

5. Zeng L, Guo Y, Liang J, Chen S, Peng P, Zhang Q, et al. Perineural Invasion and TAMs in Pancreatic Ductal Adenocarcinomas: Review of the Original Pathology Reports Using Immunohistochemical Enhancement and Relationships with Clinicopathological Features. Journal of Cancer. 2014; 5:754–60. [PubMed: 25368675]

6. Demir IE, Friess H, Ceyhan GO. Neural plasticity in pancreatitis and pancreatic cancer. Nature reviews Gastroenterology & hepatology. 2015; 12:649–59. [PubMed: 26460352]

7. He S, Chen CH, Chernichenko N, Bakst RL, Barajas F, Deborde S, et al. GFRalpha1 released by nerves enhances cancer cell perineural invasion through GDNF-RET signaling. Proceedings of the National Academy of Sciences of the United States of America. 2014; 111:E2008–17. [PubMed: 24778213]

8. Gil Z, Cavel O, Kelly K, Brader P, Rein A, Gao SP, et al. Paracrine regulation of pancreatic cancer cell invasion by peripheral nerves. Journal of the National Cancer Institute. 2010; 102:107–18. [PubMed: 20068194]

9. Deborde S, Omelchenko T, Lyubchik A, Zhou Y, He S, McNamara WF, et al. Schwann cells induce cancer cell dispersion and invasion. The Journal of clinical investigation. 2016; 126:1538–54. [PubMed: 26999607]

10. Cavel O, Shomron O, Shabtay A, Vital J, Trejo-Leider L, Weizman N, et al. Endoneurial macrophages induce perineural invasion of pancreatic cancer cells by secretion of GDNF and activation of RET tyrosine kinase receptor. Cancer research. 2012; 72:5733–43. [PubMed: 22971345]

11. Tofaris GK, Patterson PH, Jessen KR, Mirsky R. Denervated Schwann cells attract macrophages by secretion of leukemia inhibitory factor (LIF) and monocyte chemoattractant protein-1 in a process regulated by interleukin-6 and LIF. The Journal of neuroscience : the official journal of the Society for Neuroscience. 2002; 22:6696–703. [PubMed: 12151548]

12. Amit M, Na'ara S, Leider-Trejo L, Binenbaum Y, Kulish N, Fridman E, et al. Upregulation of RET induces perineurial invasion of pancreatic adenocarcinoma. Oncogene. 2017

13. Qian BZ, Li J, Zhang H, Kitamura T, Zhang J, Campion LR, et al. CCL2 recruits inflammatory monocytes to facilitate breast-tumour metastasis. Nature. 2011; 475:222–5. [PubMed: 21654748]

14. Bonapace L, Coissieux MM, Wyckoff J, Mertz KD, Varga Z, Junt T, et al. Cessation of CCL2 inhibition accelerates breast cancer metastasis by promoting angiogenesis. Nature. 2014; 515:130–3. [PubMed: 25337873]

15. Jia T, Serbina NV, Brandl K, Zhong MX, Leiner IM, Charo IF, et al. Additive roles for MCP-1 and MCP-3 in CCR2-mediated recruitment of inflammatory monocytes during Listeria monocytogenes infection. J Immunol. 2008; 180:6846–53. [PubMed: 18453605]

16. Shi C, Pamer EG. Monocyte recruitment during infection and inflammation. Nature reviews Immunology. 2011; 11:762–74.

17. He S, Chen CH, Deborde S, Bakst RL, Chernichenko N, McNamara WF, et al. The Chemokine (CCL2-CCR2) Signaling Axis Mediates Perineural Invasion. Molecular cancer research : MCR. 2015; 13:380–90. [PubMed: 25312961]

18. Demir IE, Schorn S, Schremmer-Danninger E, Wang K, Kehl T, Giese NA, et al. Perineural mast cells are specifically enriched in pancreatic neuritis and neuropathic pain in pancreatic cancer and chronic pancreatitis. PloS one. 2013; 8:e60529. [PubMed: 23555989]

19. Joyce JA, Baruch A, Chehade K, Meyer-Morse N, Giraudo E, Tsai FY, et al. Cathepsin cysteine proteases are effectors of invasive growth and angiogenesis during multistage tumorigenesis. Cancer cell. 2004; 5:443–53. [PubMed: 15144952]

20. Serbina NV, Pamer EG. Monocyte emigration from bone marrow during bacterial infection requires signals mediated by chemokine receptor CCR2. Nature immunology. 2006; 7:311–7. [PubMed: 16462739]

21. Shi C, Jia T, Mendez-Ferrer S, Hohl TM, Serbina NV, Lipuma L, et al. Bone marrow mesenchymal stem and progenitor cells induce monocyte emigration in response to circulating toll-like receptor ligands. Immunity. 2011; 34:590–601. [PubMed: 21458307]

22. Hohl TM, Rivera A, Lipuma L, Gallegos A, Shi C, Mack M, et al. Inflammatory monocytes facilitate adaptive CD4 T cell responses during respiratory fungal infection. Cell host & microbe. 2009; 6:470–81. [PubMed: 19917501]

23. Halangk W, Lerch MM, Brandt-Nedelev B, Roth W, Ruthenbuerger M, Reinheckel T, et al. Role of cathepsin B in intracellular trypsinogen activation and the onset of acute pancreatitis. The Journal of clinical investigation. 2000; 106:773–81. [PubMed: 10995788]

24. Gocheva V, Zeng W, Ke D, Klimstra D, Reinheckel T, Peters C, et al. Distinct roles for cysteine cathepsin genes in multistage tumorigenesis. Genes & development. 2006; 20:543–56. [PubMed: 16481467]

25. Shi GP, Villadangos JA, Dranoff G, Small C, Gu L, Haley KJ, et al. Cathepsin S required for normal MHC class II peptide loading and germinal center development. Immunity. 1999; 10:197–206. [PubMed: 10072072]

26. Wang Y, Zhang Y, Yang J, Ni X, Liu S, Li Z, et al. Genomic sequencing of key genes in mouse pancreatic cancer cells. Current molecular medicine. 2012; 12:331–41. [PubMed: 22208613]

27. Winograd R, Byrne KT, Evans RA, Odorizzi PM, Meyer AR, Bajor DL, et al. Induction of T-cell Immunity Overcomes Complete Resistance to PD-1 and CTLA-4 Blockade and Improves Survival in Pancreatic Carcinoma. Cancer immunology research. 2015; 3:399–411. [PubMed: 25678581]

28. Bakst RL, Lee N, He S, Chernichenko N, Chen CH, Linkov G, et al. Radiation impairs perineural invasion by modulating the nerve microenvironment. PloS one. 2012; 7:e39925. [PubMed: 22768171]

29. Ceyhan GO, Demir IE, Rauch U, Bergmann F, Muller MW, Buchler MW, et al. Pancreatic neuropathy results in "neural remodeling" and altered pancreatic innervation in chronic pancreatitis and pancreatic cancer. The American journal of gastroenterology. 2009; 104:2555–65. [PubMed: 19568227]

30. Tsou CL, Peters W, Si Y, Slaymaker S, Aslanian AM, Weisberg SP, et al. Critical roles for CCR2 and MCP-3 in monocyte mobilization from bone marrow and recruitment to inflammatory sites. The Journal of clinical investigation. 2007; 117:902–9. [PubMed: 17364026]

31. Kitamura T, Qian BZ, Soong D, Cassetta L, Noy R, Sugano G, et al. CCL2-induced chemokine cascade promotes breast cancer metastasis by enhancing retention of metastasis-associated macrophages. The Journal of experimental medicine. 2015; 212:1043–59. [PubMed: 26056232]

32. Martini R, Fischer S, Lopez-Vales R, David S. Interactions between Schwann cells and macrophages in injury and inherited demyelinating disease. Glia. 2008; 56:1566–77. [PubMed: 18803324]

33. Daniloff JK, Levi G, Grumet M, Rieger F, Edelman GM. Altered expression of neuronal cell adhesion molecules induced by nerve injury and repair. The Journal of cell biology. 1986; 103:929–45. [PubMed: 2427528]

34. Noy R, Pollard JW. Tumor-associated macrophages: from mechanisms to therapy. Immunity. 2014; 41:49–61. [PubMed: 25035953]

35. Olson OC, Joyce JA. Cysteine cathepsin proteases: regulators of cancer progression and therapeutic response. Nature reviews Cancer. 2015; 15:712–29. [PubMed: 26597527]

36. Pina-Oviedo S, Ortiz-Hidalgo C. The normal and neoplastic perineurium: a review. Advances in anatomic pathology. 2008; 15:147–64. [PubMed: 18434767]

37. Lah TT, Buck MR, Honn KV, Crissman JD, Rao NC, Liotta LA, et al. Degradation of laminin by human tumor cathepsin B. Clinical & experimental metastasis. 1989; 7:461–8. [PubMed: 2785014]

38. Buck MR, Karustis DG, Day NA, Honn KV, Sloane BF. Degradation of extracellular-matrix proteins by human cathepsin B from normal and tumour tissues. The Biochemical journal. 1992; 282(Pt 1):273–8. [PubMed: 1540143]

39. Gonzalez-Perez F, Udina E, Navarro X. Extracellular matrix components in peripheral nerve regeneration. International review of neurobiology. 2013; 108:257–75. [PubMed: 24083438]

40. Chen P, Cescon M, Bonaldo P. The Role of Collagens in Peripheral Nerve Myelination and Function. Molecular neurobiology. 2014

41. Shoji A, Kabeya M, Ishida Y, Yanagida A, Shibusawa Y, Sugawara M. Evaluation of cathepsin B activity for degrading collagen IV using a surface plasmon resonance method and circular dichroism spectroscopy. Journal of pharmaceutical and biomedical analysis. 2014; 95:47–53. [PubMed: 24631956]

42. Saloman JL, Albers KM, Li D, Hartman DJ, Crawford HC, Muha EA, et al. Ablation of sensory neurons in a genetic model of pancreatic ductal adenocarcinoma slows initiation and progression of cancer. Proceedings of the National Academy of Sciences of the United States of America. 2016; 113:3078–83. [PubMed: 26929329]

43. Rotshenker S. Wallerian degeneration: the innate-immune response to traumatic nerve injury. Journal of neuroinflammation. 2011; 8:109. [PubMed: 21878125]

44. Demir IE, Boldis A, Pfitzinger PL, Teller S, Brunner E, Klose N, et al. Investigation of Schwann cells at neoplastic cell sites before the onset of cancer invasion. Journal of the National Cancer Institute. 2014:106. [PubMed: 25174031]

45. Kalbasi A, Komar C, Tooker GM, Liu M, Lee JW, Gladney WL, et al. Tumor-Derived CCL2 Mediates Resistance to Radiotherapy in Pancreatic Ductal Adenocarcinoma. Clinical cancer research : an official journal of the American Association for Cancer Research. 2017; 23:137–48. [PubMed: 27354473]

46. Stolinski C. Structure and composition of the outer connective tissue sheaths of peripheral nerve. Journal of anatomy. 1995; 186(Pt 1):123–30. [PubMed: 7649808]

47. Bruck W. The role of macrophages in Wallerian degeneration. Brain Pathol. 1997; 7:741–52. [PubMed: 9161725]

48. Sevenich L, Bowman RL, Mason SD, Quail DF, Rapaport F, Elie BT, et al. Analysis of tumour- and stroma-supplied proteolytic networks reveals a brain-metastasis-promoting role for cathepsin S. Nature cell biology. 2014; 16:876–88. [PubMed: 25086747]

49. Niedergethmann M, Wostbrock B, Sturm JW, Willeke F, Post S, Hildenbrand R. Prognostic impact of cysteine proteases cathepsin B and cathepsin L in pancreatic adenocarcinoma. Pancreas. 2004; 29:204–11. [PubMed: 15367886]

50. Pienta KJ, Machiels JP, Schrijvers D, Alekseev B, Shkolnik M, Crabb SJ, et al. Phase 2 study of carlumab (CNTO 888), a human monoclonal antibody against CC-chemokine ligand 2 (CCL2), in metastatic castration-resistant prostate cancer. Investigational new drugs. 2013; 31:760–8. [PubMed: 22907596]

51. de Zeeuw D, Bekker P, Henkel E, Hasslacher C, Gouni-Berthold I, Mehling H, et al. The effect of CCR2 inhibitor CCX140-B on residual albuminuria in patients with type 2 diabetes and nephropathy: a randomised trial. The lancet Diabetes & endocrinology. 2015; 3:687–96. [PubMed: 26268910]

52. Li X, Yao W, Yuan Y, Chen P, Li B, Li J, et al. Targeting of tumour-infiltrating macrophages via CCL2/CCR2 signalling as a therapeutic strategy against hepatocellular carcinoma. Gut. 2015

53. Nywening TM, Wang-Gillam A, Sanford DE, Belt BA, Panni RZ, Cusworth BM, et al. Targeting tumour-associated macrophages with CCR2 inhibition in combination with FOLFIRINOX in patients with borderline resectable and locally advanced pancreatic cancer: a single-centre, open-label, dose-finding, non-randomised, phase 1b trial. The Lancet Oncology. 2016
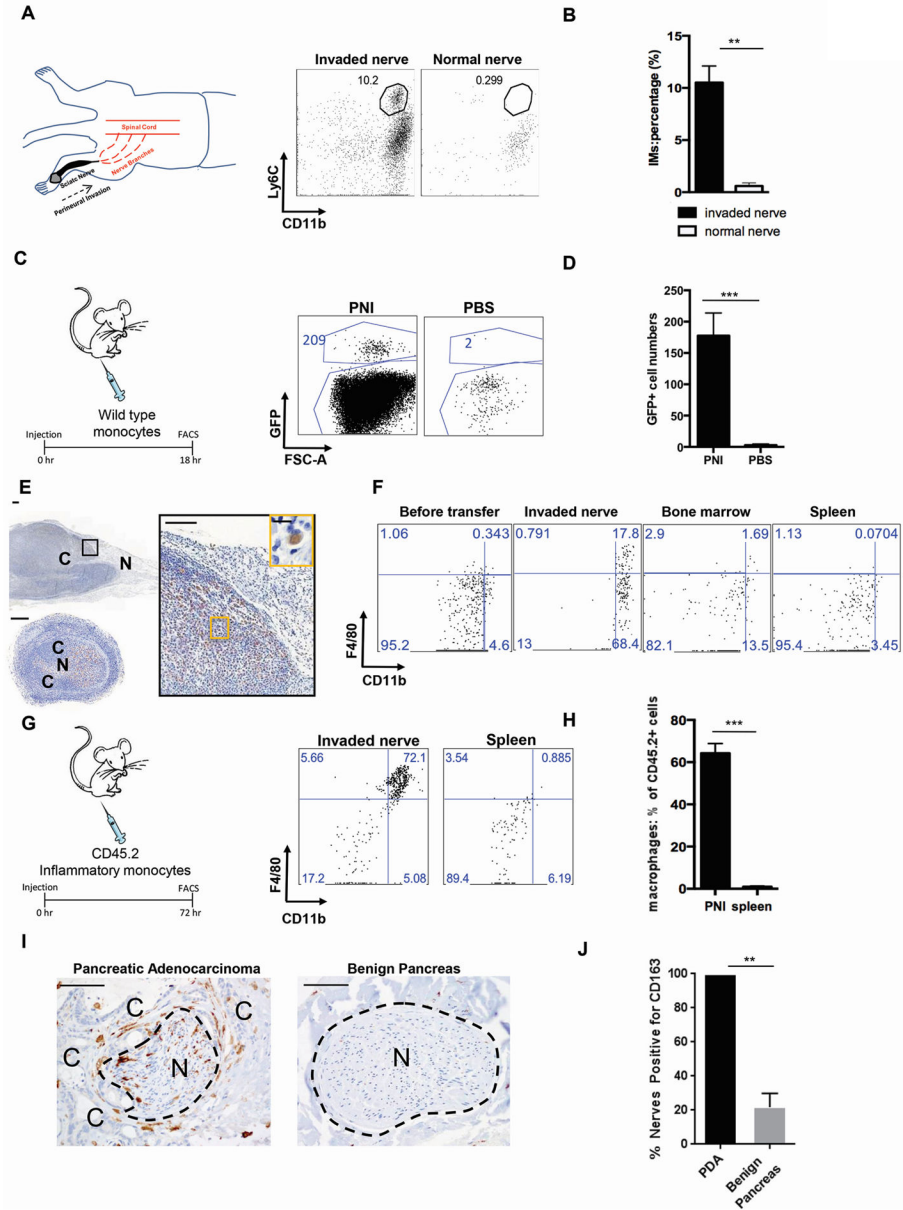
Figure 1. Nerves invaded by cancer recruit inflammatory monocyte-derived macrophages

A, Left, Schematic for our *in-vivo* model of PNI in which cancer is injected into the distal sciatic nerve and invades unidirectionally towards the spinal cord, resulting in hind limb paralysis. Right, Representative flow cytometry diagrams showing expression of Ly6C and CD11b of endogenous IM isolated from an invaded and normal murine sciatic nerve one week following cancer injection. **B,** Quantification of percentage of IM among CD45^{+} cells by flow cytometry in a murine model of PNI. Data shown as mean + s.e.m., $n = 3$; **, P=. 003, unpaired t-test. **C,** Left, schematic for the adoptive transfer of green fluorescent protein positive (GFP+) IM into mice with nerve invasion. Right, Representative flow diagrams from invaded (PNI) and control nerve (PBS) specimens showing the amount of GFP^{+} cells isolated 18 hours after adoptive transfer of GFP[+] IM. Absolute number of GFP^{+} cells are

shown in blue. PBS, Phosphate buffered saline. **D,** Absolute numbers of donor IM recruited to invaded and control nerves. Data shown as mean + s.e.m., $n = 3$; ***, P<.001, unpaired t-test. **E,** Representative longitudinal (top) and cross-sectional (bottom) images of anti-GFP stained invaded nerve from (C). Inset from longitudinal image. C, indicates cancer. N, indicates nerve. Scale bar 200 μm, inset 10 μm. **F,** Representative flow cytometry plots showing expression of F4/80 and CD11b of transferred IM pre- and post-transfer. Macrophage differentiation (F4/80+ CD11b+) is only observed in the invaded nerve. **G,** Left, schematic for adoptive transfer of CD45.2 WT IM into a CD45.1 WT mouse with nerve invasion. Right, Representative flow diagram of CD45.2+ cells isolated from an invaded sciatic nerve and spleen 72 hours following adoptive transfer into CD45.1+ WT mouse. Macrophage differentiation (CD11b+ F4/80+) is only seen in the invaded nerve. **H,** Quantification of CD45.2+ macrophages isolated from invaded nerves and respective spleens. Data shown as mean + s.e.m., $n = 3$; ***, P=0.0002, unpaired t-test. **I,** Representative images of anti-CD163 staining in human PDA and benign pancreas. C, indicates cancer. N, indicates nerve. Scale bar 100 μm. **J,** Quantification of anti-CD163 staining intensity per nerve expressed as a score for PDA and benign pancreas ($n = 5$ in each group). Percentage of nerves positive for anti-CD163. Data shown as mean + s.e.m.. **, P=. 0079, unpaired t-test.
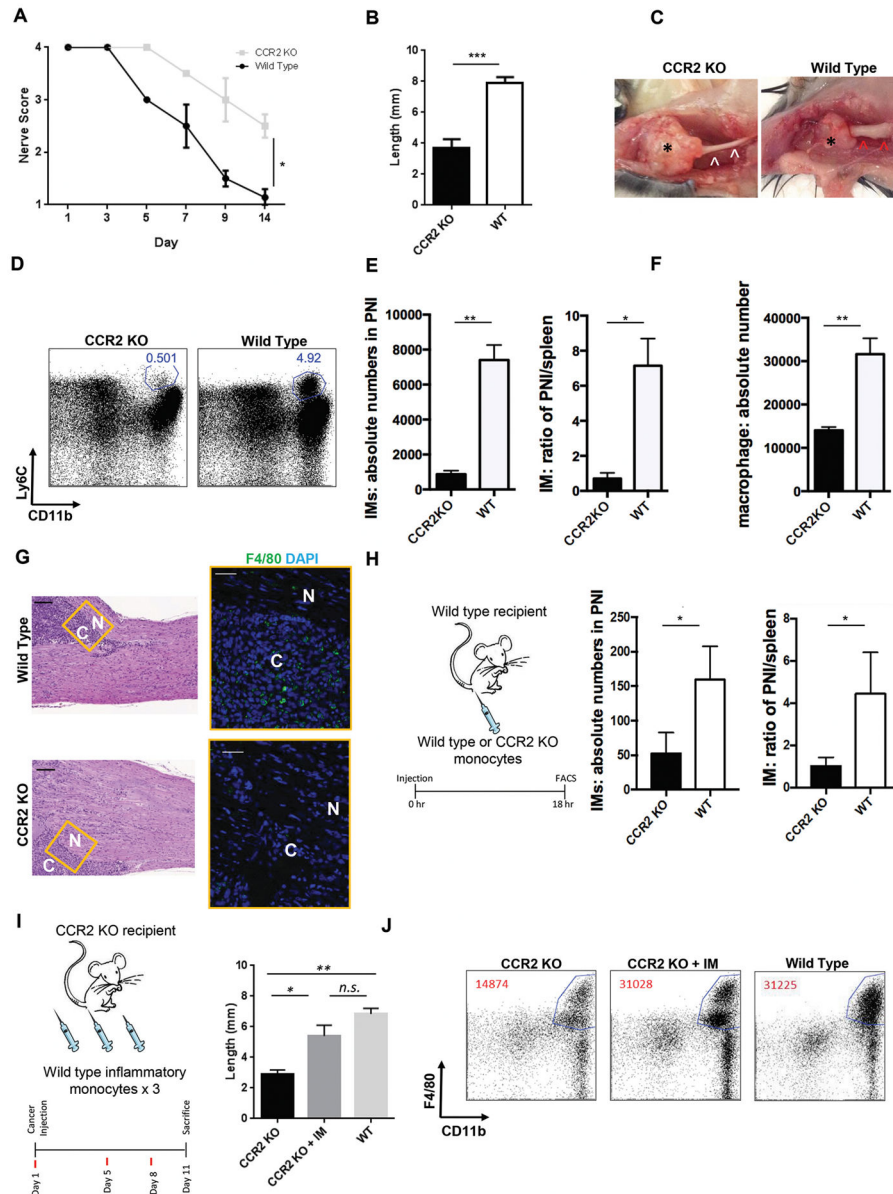
Figure 2. CCR2-expressing inflammatory monocytes promote perineural invasion

A, Nerve function scores for WT and CCR2 KO mice. Data are shown as means ± s.e.m., *n* = 7 per group; *, P<0.05, Mann Whitney test. **B,** Length of invasion for the same cohort as (A). Data are shown as means + s.e.m.. ***, P<0.001, unpaired t-test. **C,** Representative images of gross nerve specimens from WT and CCR2 KO mice; * Indicates the primary tumor, red arrowheads indicate the adjacent thickened invaded nerve, and white arrowheads indicate a thin uninvaded nerve. **D,** Representative flow diagrams from CCR2 KO and WT mice showing expression of Ly6C and CD11b of endogenous IM recruited to sciatic nerves following Panc02 injection. **E,** Left, absolute numbers of endogenous IM isolated from CCR2 KO and WT nerve specimens. Right, relative amounts of IM normalized to the splenic population. Data are shown as means + s.e.m., *n* = 3 per group; *, P<0.05, **,

P<0.01, unpaired t-test. **F,** Absolute numbers of macrophages isolated from same cohort as (E). Data are shown as means + s.e.m.. **, P<0.01, unpaired t-test. **G,** Representative images of anti-F4/80 staining (green) adjacent to cancer (C) invasion along the nerve (N). Black scale bar 100 μm, white scale bar 50 μm. **H,** Left, schematic for adoptive transfer of WT or CCR2 KO IM into WT mice with nerve invasion. Middle, absolute numbers of CCR2 KO and WT IM isolated from nerves. Right, relative amounts of IM normalized to the splenic population. Data are shown as means + s.e.m., n = 3 per group; *, P<0.05, unpaired t-test. **I,** Left, schematic for the sequential adoptive transfers of WT IM into CCR2 KO mice at days 1, 5, 8. Right, length of invasion for respective cohorts. Data are shown as means + s.e.m., n = 2 per group; *, P<0.05, **, P<0.01, unpaired t-test. **J,** Representative flow cytometry plots showing expression of F4/80 and CD11b among CD45+ cells in the sciatic nerve specimens from the respective cohorts. Cell numbers in the macrophage gate (F4/80$^+$CD11b$^+$) are indicated in red.
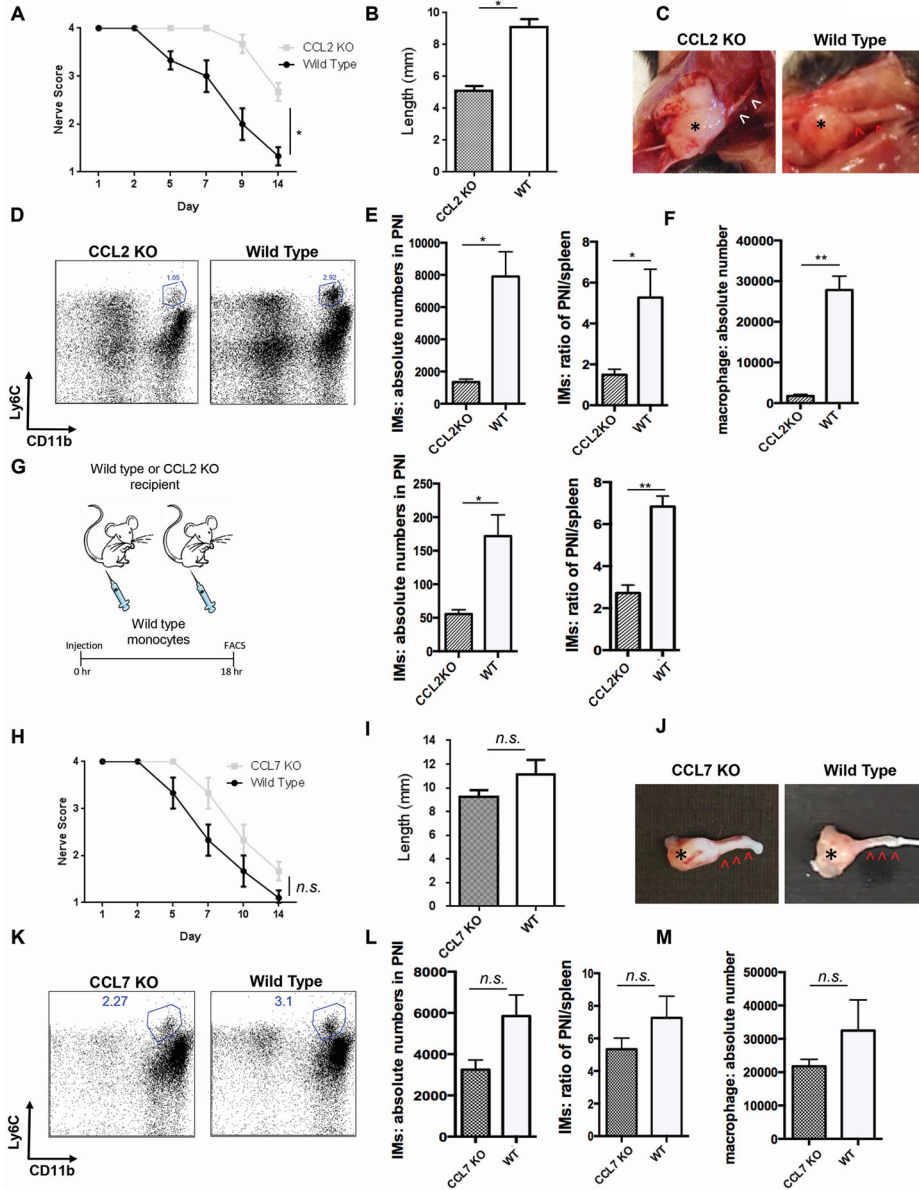
Figure 3. Loss of CCL2 but not CCL7 impairs PNI *In Vivo*.
A, Nerve function scores for WT and CCL2 KO mice. Data are shown as means ± s.e.m., *n* = 5 per group; *, P<0.05, Mann Whitney test. **B,** Length of invasion for the same cohort as (A). Data are shown as means + s.e.m.. *, P<0.05, unpaired t-test. **C,** Representative gross images of nerves from WT and CCL2 KO mice; * Indicates the primary tumor, red arrowheads indicate the adjacent thickened invaded nerve, and white arrowheads indicate a thin uninvaded nerve. **D,** Representative flow cytometry plots showing expression of Ly6C and CD11b of endogenous IM recruited to sciatic nerves following cancer injection. **E,** Left, absolute numbers of endogenous IM isolated from CCL2 KO and WT nerve specimens. Right, relative amounts of IM normalized to the splenic population. Data are shown as means + s.e.m., *n* = 5 per group; *, P<0.05, unpaired t-test. **F,** Absolute numbers of

macrophages isolated from same cohort as (E). **, P<0.01, unpaired t-test. **G**, Left, schematic for the adoptive transfer of IM into WT or CCL2 KO mice following cancer injection. Middle, absolute numbers of WT or CCL2 KO IM isolated from nerves. Right, relative amounts of IM normalized to the splenic population. Data are shown as means + s.e.m., $n = 4$ per group; *, P<0.05, **, P<0.01, unpaired t-test. **H**, Nerve function scores for CCL7 KO and WT mice following cancer injection. Data are shown as means + s.e.m., $n = 6$ per group; P=0.24, Mann Whitney test. n.s. not significant. **I**, Length of invasion for the same cohort as (H). Data are shown as means + s.e.m.. P=0.10, unpaired t-test. n.s. not significant. **J**, Representative gross images of nerves from CCL7 KO and WT mice. * Indicates the primary tumor, red arrowheads indicate the adjacent thickened invaded nerve. **K**, Representative flow cytometry plots showing expression of Ly6C and CD11b of endogenous IM recruited to CCL7 KO and WT nerves following cancer injection. **L**, Left, absolute numbers of endogenous IM isolated from CCL7 KO and WT nerve specimens. Right, relative amounts of IM normalized to the splenic population. Data are shown as means + s.e.m., $n = 6$ per group; P=0.11 and 0.26 respectively. n.s. not significant. **M**, Absolute numbers of macrophages isolated from same cohort as (L). Data are shown as means + s.e.m.. P=0.28, unpaired t-test. n.s. not significant.
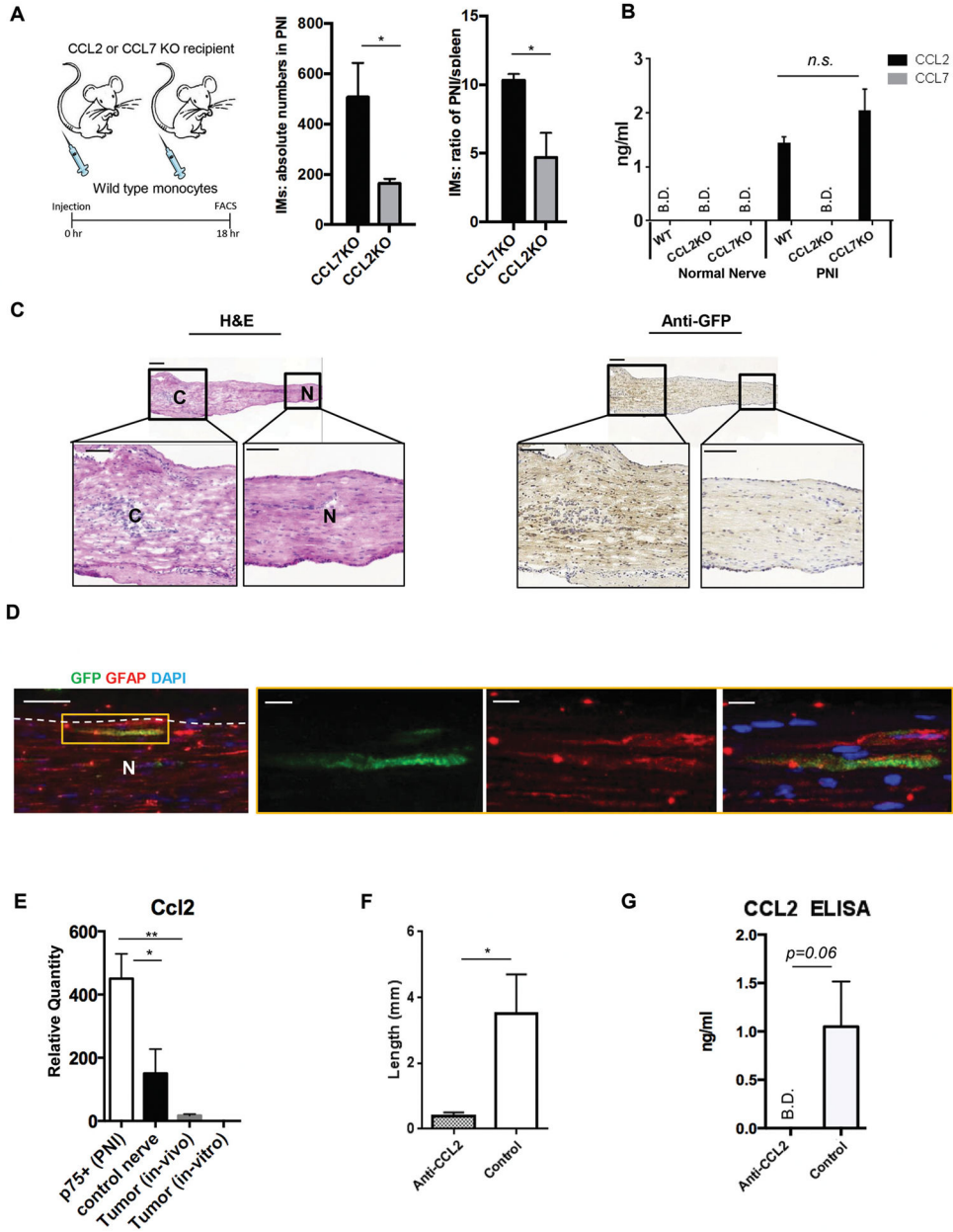
Figure 4. Schwann cell secreted CCL2 drives inflammatory monocyte recruitment to invaded nerves

A, Left, schematic for the adoptive transfer of WT IM into CCL2 KO or CCL7 KO following cancer injection. Middle, absolute numbers of IM isolated from CCL7 KO or CCL2 KO nerves. Right, relative amounts of IM normalized to the splenic population. Data are shown as means + s.e.m., $n = 4$ per group; *, P<0.05, unpaired t-test. **B,** CCL2 and CCL7 ELISA from CCL2 KO, CCL7 KO, and WT nerve lysates following cancer injection. Data are shown as means + s.e.m, $n = 3$ per group; P=0.27, unpaired t-test. B.D., below detection. n.s., not significant. **C,** Left, representative images of H&E staining of invaded nerves (N) in CCL2-green fluorescent protein (GFP) reporter mice. Right, the same section stained for

anti-GFP demonstrating staining in regions of cancer (C) and decreased staining farther from regions of invasion in normal nerve (N). Scale bar 100 μm. **D,** Representative image of an invaded nerve (N) from CCL2-GFP reporter mice stained for anti-GFAP (red) and anti-GFP staining (green). Dotted line delineates upper nerve border. Scale bar 50 μm, inset 10 μm. **E,** *Ccl2* RT-PCR performed on FACS-sorted Schwann cells (p75+) from invaded (PNI) and control nerves, Panc02 isolated from *in vivo* tumors and *in vitro*. Data are shown as means + s.e.m, $n = 4, 4, 2, 2$, respectively. *, P<0.05. **, P<0.01, unpaired t-test. **F,** Length of nerve invasion following treatment with daily anti-CCL2 antibody or control. Data are shown as means + s.e.m., $n = 4$ per group; *, P<0.05, unpaired t-test. **G,** CCL2 ELISA performed on nerve lysates for the same cohort as (F). B.D. below detection.
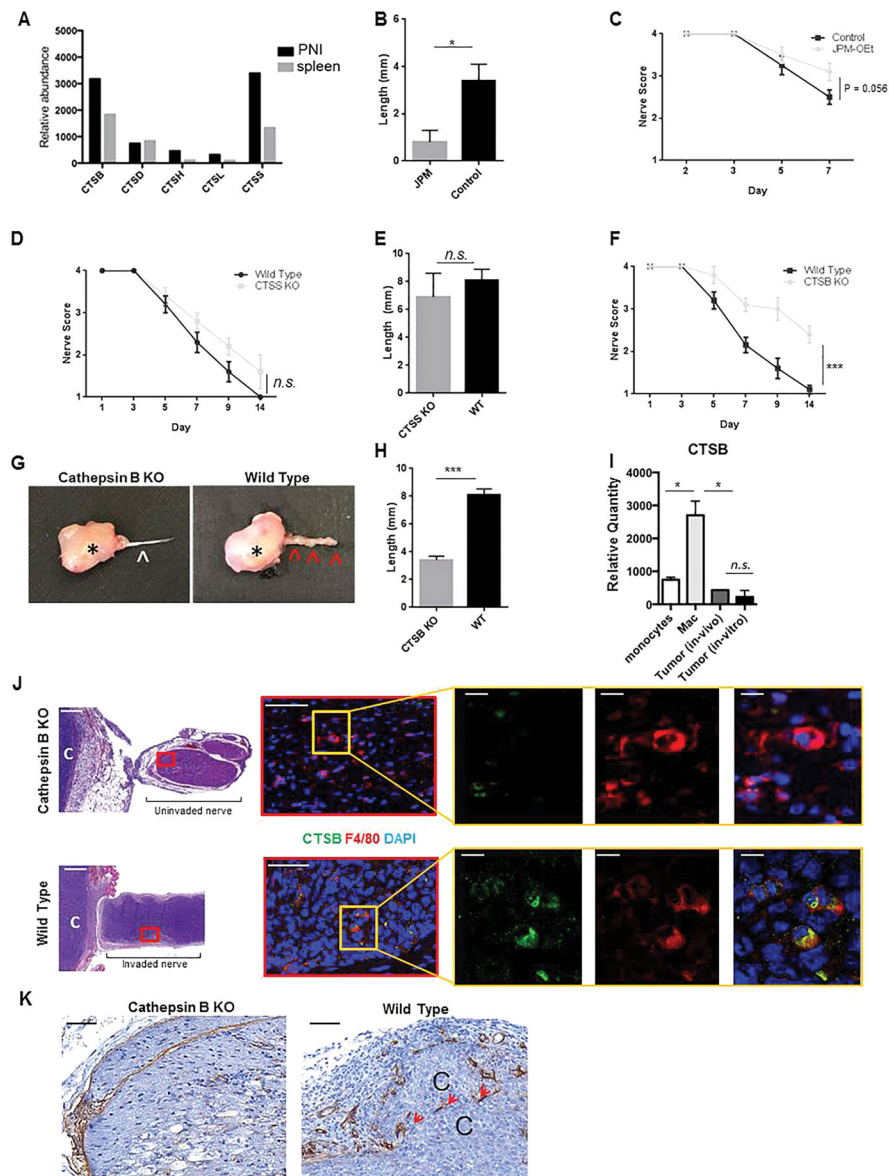
Figure 5. Macrophage derived cathepsin B promotes perineural invasion

A, RT-PCR performed on macrophages isolated from invaded *in vivo* nerve specimens and respective spleens for members of the cathepsin protease family. **B,** Length of invasion following treatment with JPM-OEt, a pan-cathepsin inhibitor. Data are shown as means + s.e.m., *n* = 10 per group; *, P<0.05, unpaired t-test. **C,** Nerve function scores for same cohort as (B). Mann Whitney test. **D,** Nerve function scores for WT and CTSS KO. Data are shown as means ± s.e.m., *n* = 5 per group; P=0.44, Mann Whitney test. n.s. not significant. **E,** Length of invasion for the same cohort as (D). Data are shown as means + s.e.m.. P=0.61. n.s., not significant. **F,** Nerve function scores for WT and CTSB KO. Data are shown as means ± s.e.m., *n* = 10 per group; ***, P=0.0004, Mann Whitney test. **G,** Representative gross images of nerves from CTSB KO and WT mice. * Indicates the primary tumor, red arrowheads indicate the adjacent thickened invaded nerve, and white arrowheads indicate a

thin uninvaded nerve. **H,** Length of invasion for the same cohort as (G). Data are shown as means + s.e.m.. ***, P<0.001, unpaired t-test. **I,** *Ctsb* RT-PCR performed on IM, macrophages, and Panc02 isolated from *in vivo* nerve specimens. $n = 6, 6, 2, 2$, respectively; *, P< 0.05, unpaired t-test. n.s. not significant. **J,** Representative images of H&E stained sections of WT and CSTB KO nerves. Scale bar, 200 μm with corresponding images of adjacent sections co-stained for anti-CTSB (green) or anti-F4/80 (red). Scale bar 50 μm, insert 10 μm. **K,** Representative images of anti-collagen IV staining in CTSB and WT nerves specimens. Red arrowheads delineate collagen IV irregularity. C indicates cancer. Scale bar 50 μm.
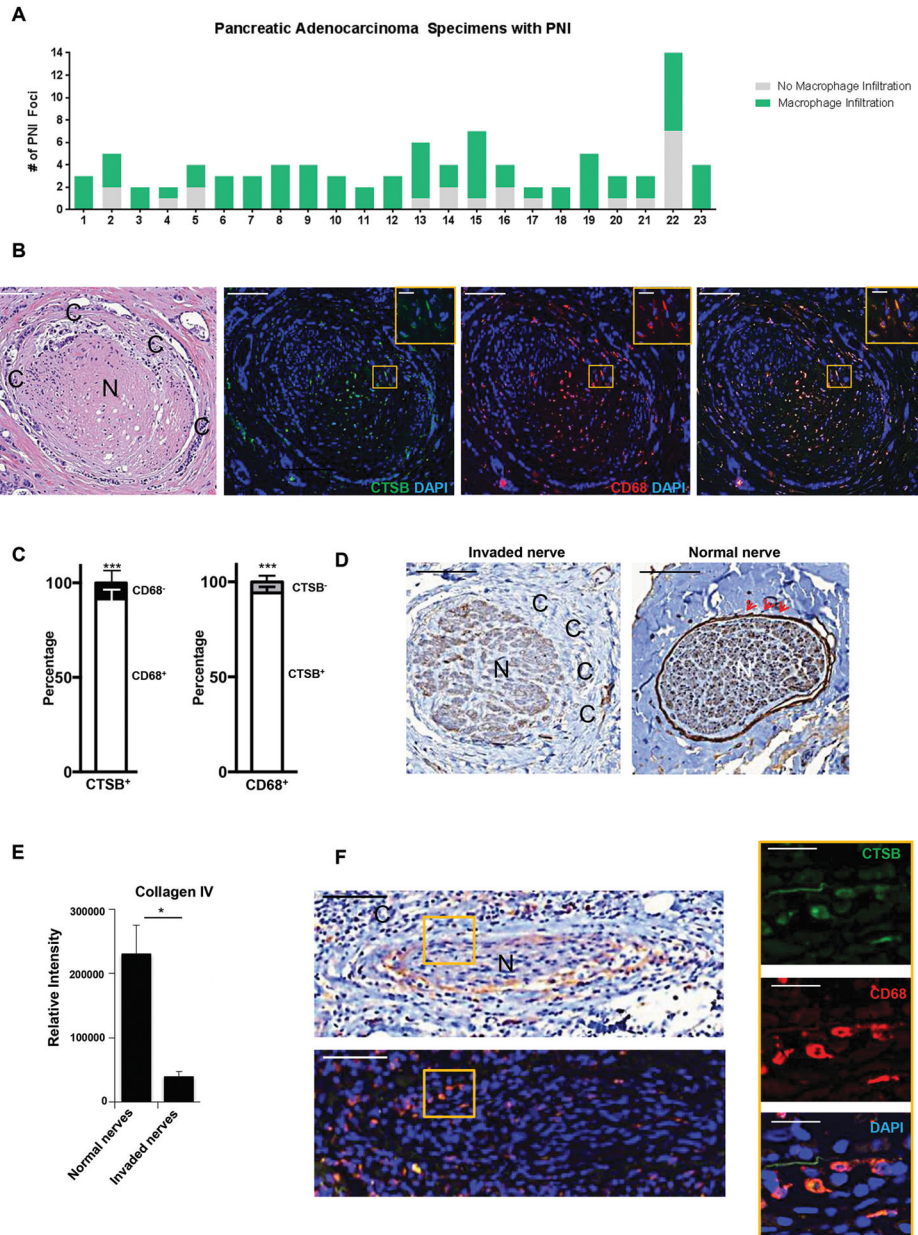
Figure 6. Disruption of the perineurium is associated with cathepsin B expressing macrophages in human tumors

A, Frequency of macrophage infiltration by anti-CD163 staining along individual nerve foci with PNI in human PDA. **B,** Representative images of H&E staining of human PDA specimens with PNI with adjacent specimens stained for anti-CTSB (red) and anti-CD68 (green). Scale bar 100 μm, inset 10 μm. C, indicates cancer. N, indicates nerve. **C,** Co-expression analysis of individual cells from regions of PNI in human PDA specimens stained for anti-CD68 and anti-CTSB. Data are shown as means + s.e.m., *n* = 10 PDA specimens. ***, P<0.001, unpaired t-test. **D,** Representative images of normal nerves from benign pancreas and invaded nerves from PDA stained for anti-collagen IV. Scale bar 100

µm. Red arrowheads delineate the outer border of a normal nerve, comprised of collagen IV. C, indicates cancer. N, indicates nerve. **E,** Quantification of anti-collagen IV staining intensity. Data are shown as means + s.e.m.. $n = 31$ normal nerves and $n = 26$ invaded nerves from 10 specimens; *, P<0.05, unpaired t-test. **F,** Left top, representative images of anti-collagen IV stating of human PDA with PNI; left bottom, adjacent sections stained for anti-CTSB (green) and anti-CD68 (red). Right, high power image demonstrating CTSB expressing macrophages are present adjacent to regions of disrupted anti-collagen IV staining. Scale bar 50 µm, inset 25 µm. C, indicates cancer. N, indicates nerve.
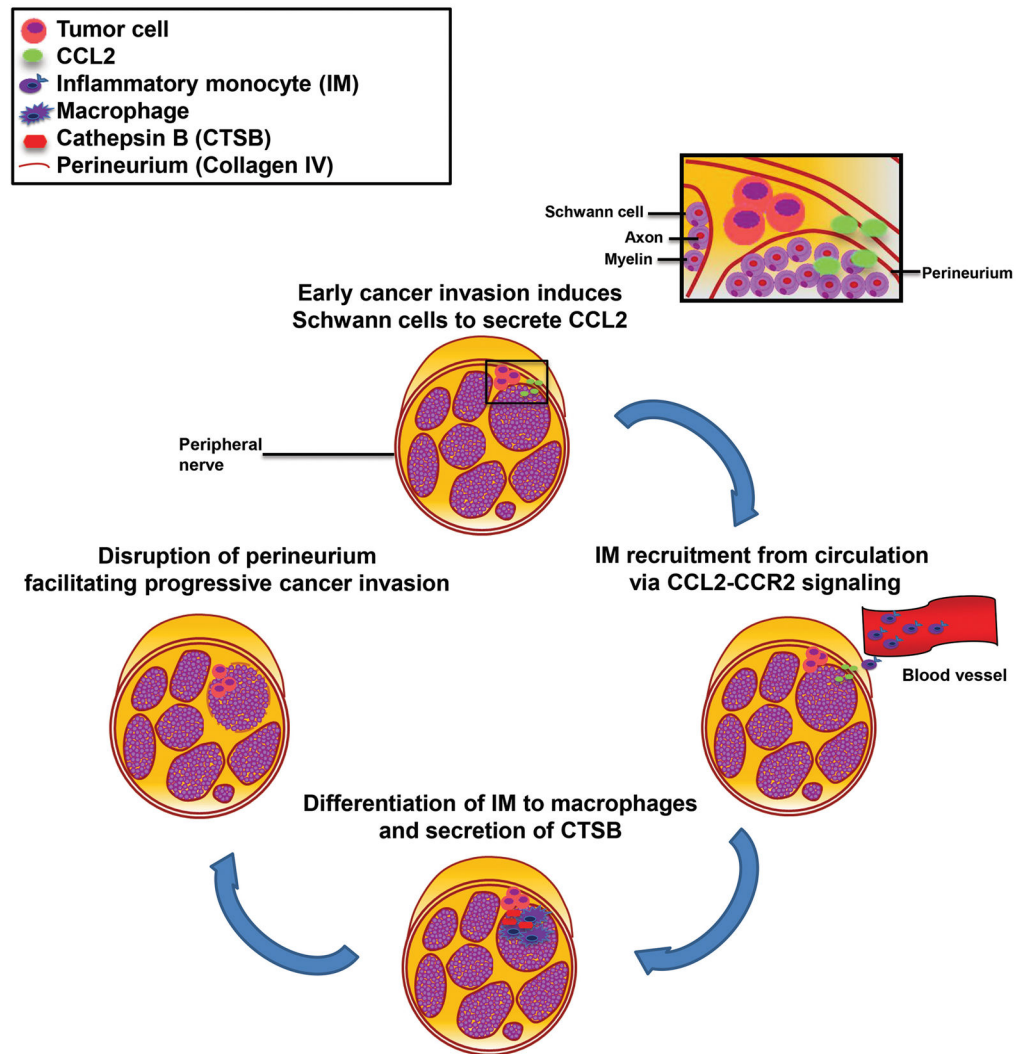
Figure 7. Summary diagram

The data from this study support the model that in the presence of cancer, Schwann cells secrete CCL2 and recruit inflammatory monocytes (IM) from the circulation via CCR2, which facilitates tumor invasion into and along the nerve through a cathepsin B mediated disruption of the protective perineurium.